

Time resolution studies for the future LHCb Electromagnetic Calorimeter

Alberto Bellavista^{a,b,*} on behalf of the LHCb ECAL Upgrade II R&D group

^a*Physics Department, University of Bologna,
via Irnerio 46, Bologna, Italy*

^b*INFN Bologna*

E-mail: alberto.bellavista@bo.infn.it

During Runs 5 and 6 of the Large Hadron Collider (LHC), the LHCb experiment at CERN will operate at a luminosity up to $1.5 \times 10^{34} \text{ cm}^{-2} \text{ s}^{-1}$, requiring substantial upgrades to its Electromagnetic Calorimeter (ECAL). Specifically, the upgraded detector will have to withstand high radiation doses and achieve time resolutions of a few tens of picoseconds in order to mitigate pile-up effects.

The inner and high-occupancy regions of the future detector — named PicoCal — will utilize a new Spaghetti-Calorimeter (SpaCal) technology composed of scintillating fibres (polystyrene or garnet crystals) in a dense absorber (lead or tungsten). Ongoing investigations are focused on the photodetectors (PMTs) selection and their impact on the overall timing performance.

Simulation studies of a lead-polystyrene module with single-sided readout (PMTs coupled only to the downstream side) show that fast PMTs result in worse time resolutions due to the longitudinal showers' fluctuations, which introduce a bias in the timestamps determined by the Constant Fraction Discriminator (CFD) algorithm. This hypothesis was corroborated by observing that a significant improvement in time resolution would be achievable if the positions of the electromagnetic shower barycenters were known. Additionally, a correlation between signal rise time and depth of the electromagnetic showers has been observed.

Data from a test beam campaign conducted at the CERN SPS in June 2024 have been analysed to measure the time resolution of a tungsten-polystyrene SpaCal prototype, comparing four PMT models and two fibre types. By exploiting a rise-time-based correction procedure, time resolutions below 20 ps at high energies have been reached, with the fastest PMTs undergoing larger corrections, as expected from simulations.

*Third Italian Workshop on the Physics at High Intensity (WIFAI2024)
12-15 November 2024
Bologna, Italy*

*Speaker

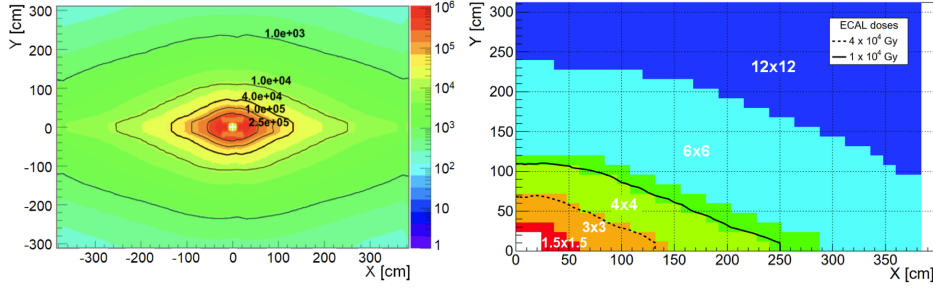


Figure 1: (Left) Absorbed radiation dose (in Gray) expected for the LHCb PicoCal modules by the end of their operation, depending on their position on the PicoCal surface [4]. (Right) Cells sizes (in cm) in the different PicoCal regions [2].

1. Introduction

To fully exploit the physics potential offered by the high-luminosity phase of the LHC [1], the LHCb experiment will undergo a second major upgrade (LHCb Upgrade II), scheduled for the fourth long shutdown of the LHC (LS4). Starting from the subsequent Run 5 of the LHC, the LHCb experiment will operate at a peak luminosity of $1.5 \times 10^{34} \text{ cm}^{-2} \text{ s}^{-1}$. To handle the high particle flux, a significant upgrade of the Electromagnetic Calorimeter (ECAL) is required to withstand radiation doses up to 1 MGy in its innermost region. The upgraded ECAL, known as PicoCal, must also deliver precise timing information to reduce pile-up effects, achieving time resolutions in the order of tens of picoseconds [2]. Additionally, its energy resolution must remain consistent with the current performance, i.e. $\frac{\sigma(E)}{E} \sim \frac{10\%}{\sqrt{E}} \oplus 1\%$.

Currently, the LHCb ECAL is composed of Shashlik modules presenting 4 mm plastic scintillator tiles alternated with 2 mm thick lead plates [3]. The novel detector technology under development is a Spaghetti Calorimeter (SpaCal) composed of scintillating fibres (polystyrene or garnet crystal) inserted in a dense and passive absorber (lead or tungsten). The light produced by the incident particles inside the fibres will be read out by photomultiplier tubes (PMTs). The baseline configuration of the PicoCal after LS4 involves SpaCal-W modules with tungsten absorber and radiation-hard inorganic crystal fibres in the innermost region. Then, a middle region will be composed of lead absorber and polystyrene plastic fibres (Spacal-Pb). The outer region will be equipped with Shashlik modules of various granularities. Each module will be segmented longitudinally into a front (upstream) and back (downstream) section, with a mirror between the two parts and PMTs placed in correspondence of both sides (double-sided readout). Depending on their granularity and radiation-hardness capabilities, the modules will be arranged in rhomboidal regions matching the map of occupancy and absorbed dose on the PicoCal surface [2], as illustrated in Fig. 1.

During LS3 an enhancement of the detector is required, replacing the innermost Shashlik modules with SpaCal-W and SpaCal-Pb ones equipped with polystyrene fibres [5]. Such modules will be installed in a single-sided readout mode, having a unique section equipped with PMTs on the downstream face and a mirror on the upstream one to enhance the collected photostatistics. This configuration is more economically advantageous compared to the double-sided readout one.

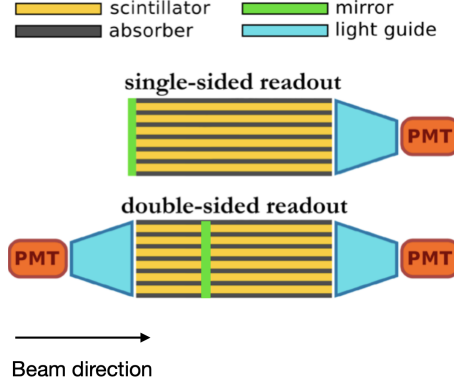


Figure 2: Schematic comparison between a SpaCal module in single-sided (top) and double-sided (bottom) readout configurations.

Consequently, there are ongoing discussions about the feasibility of using such modules beyond LS4, provided they meet the Upgrade II requirements. A schematic comparison between these two types of modules is illustrated in Fig. 2.

In the following, time resolution studies of single-sided readout modules are discussed. First, simulation analyses of a Pb-Polystyrene module are presented. Then, measurements from a testbeam campaign at the CERN SPS in June 2024 are reported.

2. Simulation studies of a Pb-Polystyrene module

Simulations of a Pb-Polystyrene module [4] in single-sided readout configuration have been performed, studying the time resolution as a function of the PMTs response celerity with 1 GeV and 10 GeV incident electrons. The PMT was simulated parametrically, modelling its single photoelectron pulse as

$$f(t) = 10^9 \cdot \frac{R \cdot \text{gain} \cdot q_e}{\tau^3} \cdot t^2 \cdot e^{-t/\tau}, \quad (1)$$

with $R = 50 \, \Omega$, $q_e = -1.6 \times 10^{-19} \, \text{C}$ and t and τ expressed in ns. The main parameter influencing the time resolution resulted to be τ (varied between 0.1 ns and 2 ns), which is proportional to the Full Width at Half Maximum (FWHM) of the pulse and thus represents the celerity of the PMT response. In the following results, the simulated gain was 10^4 .

The timestamp of the pulses generated by incident electrons is determined using the Constant Fraction Discriminator (CFD) algorithm. This algorithm identifies the moment when the signal surpasses a specified fraction of its amplitude, optimized to achieve the best overall time resolution. The time resolution is defined as the standard deviation of the sample of timestamps.

As expected, 10 GeV electrons yield lower time resolution compared to the 1 GeV case. Additionally, slower PMTs (higher τ) perform better than faster ones (lower τ). This improvement is attributed to slower PMTs being less affected by the longitudinal fluctuations of the electromagnetic showers within the detector [6]. In fact, shower depth (defined as the energy-weighted average of the longitudinal position of the energy deposits inside the fibers) and CFD timestamp are two correlated variables. For deeper showers:

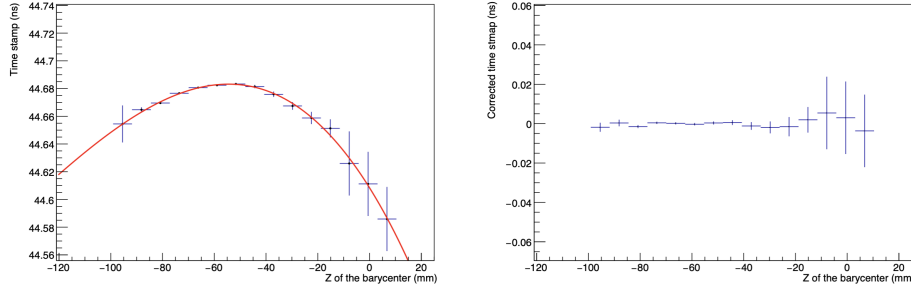


Figure 3: Example of the correction procedure removing the shower depth bias. (Left) Profiled scatter plot of the CFD timestamp vs the shower depth, with the best-fit correction function overlaid. (Right) Same, but using the unbiased timestamp instead of the original one (i.e. after applying the correction).

- direct photons (i.e. the ones produced by the scintillation process towards the readout section) arrive earlier on average, causing a negative correlation;
- reflected photons arrive later on average, producing a positive correlation.

These effects are more relevant for fast PMTs, since they are better able to distinguish between direct and reflected photons, and eventually affect the shape of the readout signals. The CFD algorithm is not able to take shape variations into account, leading to a degradation of the time resolution. In addition, they depend on the chosen CFD threshold: lower (higher) thresholds mainly depend on direct (reflected) photons, while for some intermediate choices the two correlations cancel out each other, partially removing the overall bias.

A preliminary procedure aiming at removing the shower depth bias has been developed. It consists in finding a calibration curve (f) by means of a polynomial fit to the (profiled) scatter plot of timestamp depending on the shower depth. For the j^{th} event, the corrected timestamp can be defined as $\hat{t}_j \doteq t_j - f_j$, where t_j is the original CFD timestamp and f_j represents the fit function evaluated at the corresponding shower depth. An example of the procedure is illustrated in Fig.3, where the bias removal is clearly visible. When applying this procedure, the optimal CFD threshold may be different compared to the case in which the bias is not removed. The corrected time resolution is then defined as the standard deviation of the corrected timestamps sample.

As it can be observed in Fig. 4, the time resolution obtained with fast PMTs (low τ) undergoes wider corrections and becomes less τ -dependent after applying the above-described procedure. Moreover, the best CFD threshold resulted to be always either 10% or 90% since in these cases the correlation between timestamp and shower depth is maximum, leading to the most effective corrections.

3. Analysis of testbeam data

A testbeam campaign at the CERN SPS has been conducted in June 2024, characterizing several SpaCal and Shashlik prototypes with incident electrons and hadrons beams between 20 GeV and 100 GeV. Here, time resolution measurements of a SpaCal-W module equipped with polystyrene

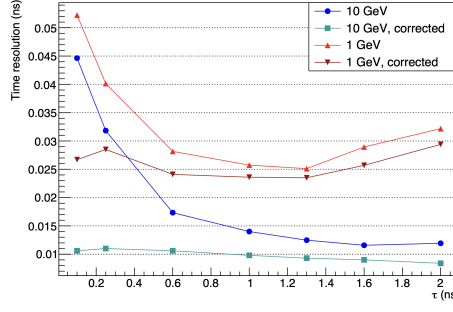


Figure 4: Time resolution before and after the bias correction as a function of τ , for 1 GeV and 10 GeV simulated incident electrons. The CFD threshold is chosen as the one which minimises the time resolution for each point. Here, electronic noise and amplitude fluctuations of the PMT pulses were set to zero in order to avoid extra contributions to the resolution.

fibres and impinged by electron beams¹ are presented. The module is composed of 4 cells, $2 \times 2 \text{ cm}^2$ each. A comparison between two different kinds of fibres (Kuraray SCSF-78 and 3HF emitting blue and green light, respectively) and four candidate PMT models (Hamamatsu R14755U-100, R9880U-20, R7600U-20 and R11187) has been performed.²

The measured time resolution as a function of the incident electrons' energy is shown in Fig. 5, comparing the results of the four PMTs under test. In all PMT cases, the SCSF-78 fibers show better results compared to the 3HF ones, since they feature faster decay times of the scintillation kinetics. In addition, slower PMTs (R7600U-20 and R11187) perform better with this fibre type, as expected from simulations. Conversely, when equipping 3HF fibres the best results are obtained with the PMTs featuring an Extended Red Multi Alkali photocathode (R7600U-20, R9880U-20), i.e. with enhanced quantum efficiencies in the green wavelength regime.

Simulations show that the shower depth is highly correlated with the rise time of the signals. Therefore, it is possible to apply the procedure described in the previous section by exploiting the latter instead of the depth of the shower's barycentre, which is not known. The time resolution measured with the fastest PMTs (R14755U-100 and R9880U-20) undergoes wider corrections. As shown in Fig. 6, resolutions below 20 ps at high energies have been obtained, with the best results given by SCSF-78 fibres and R7600U-20 PMT.

4. Conclusions

Simulation studies and testbeam data analyses of SpaCal modules in single-sided readout mode have been conducted. Specifically, the time resolution obtained with incident electrons have been measured, focusing on how the longitudinal fluctuations of the electromagnetic showers may affect the results.

¹hitting the prototype in the centre of one cell

²The PMTs were coupled to the fibers through a 5-cm long light guide; a delayed-wire-chamber detector was used to select electrons impinging onto a $10 \times 10 \text{ mm}^2$ area in the cell centers; the reference time was provided by two microchannel-plate detectors (MCPs), whose combined time resolution was about 15 ps; signals were digitized using the DRS4-based V1742 CAEN digitizer with 5 GS/s. Contributions from reference time and electronic noise are always subtracted from the time-resolution results reported in this proceeding.

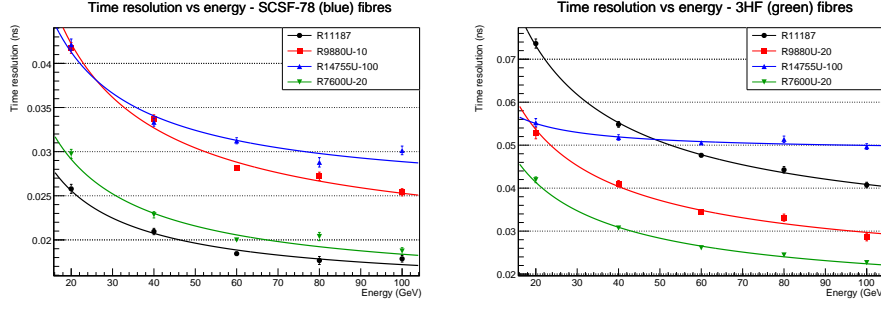


Figure 5: Measured time resolution as a function of the incident electrons' energy, with the corresponding error bars. The fit function is described by the quadrature sum of a sampling (s) and a constant (c) term: $\sigma_t(E) = s/\sqrt{E} \oplus c$. For the four PMTs under test, SCSF-78 (left) or 3HF (right) scintillating fibres were employed.

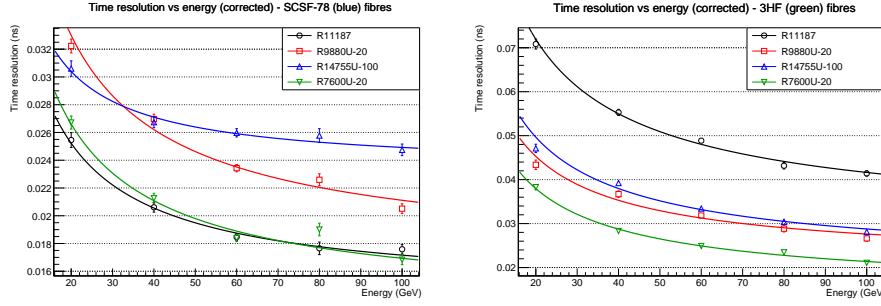


Figure 6: Measured time resolution as a function of the incident electrons' energy, with the corresponding error bars, after the correction procedure. The fit function is described by the quadrature sum of a sampling (s) and a constant (c) term: $\sigma_t(E) = s/\sqrt{E} \oplus c$. For the four PMTs under test, SCSF-78 (left) or 3HF (right) scintillating fibres were employed.

Simulations showed that the CFD timestamp is biased by the showers depth, thus worsening the time resolution. A correction procedure have been developed in order to remove such bias. Faster PMTs resulted to be more affected by these effects, leading to a variation of the readout signals' shape which can't be taken into account by the CFD algorithm.

Data collected during a testbeam campaign in June 2024 have been analysed, comparing four candidate PMT models and two kinds of polystyrene fibres. The correction procedure has been applied exploiting the rise time of the signals as a proxy for the shower depth. Such a method was found to be effective and promising for the PicoCal R&D. Resolutions below 20 ps at energies above 80 GeV have been obtained, proving the good timing capabilities of the SpaCal modules even in a single-sided readout configuration.

5. Acknowledgements

The work contained in this paper is supported by the Italian Ministero dell'Università e Ricerca (MUR) and European Union - Next Generation EU through the research grant number

2022MHC2MH, CUP I53D23001310006, under the program PRIN 2022.

References

- [1] LHCb Collaboration. Physics case for an LHCb Upgrade II - Opportunities in flavour physics, and beyond, in the HL-LHC era. Technical report, CERN, Geneva, 2016. ISBN 978-92-9083-494-6.
- [2] LHCb collaboration. LHCb Particle Identification Enhancement Technical Design Report. Technical report, CERN, Geneva, 2023.
- [3] LHCb Collaboration. The lhcb detector at lhc. *JINST*, 2008.
- [4] LHCb Collaboration. Framework TDR for the LHCb Upgrade II: Opportunities in flavour physics, and beyond, in the HL-LHC era. Technical report, CERN, Geneva, 2021.
- [5] Sergei Kholodenko. Scintillating sampling ECAL technology for the LHCb PicoCal. *Nucl. Instrum. Methods Phys. Res., A*, 1066:169656, 2024.
- [6] Alberto Bellavista. Study of the simulations of the readout for the future lhcb electromagnetic calorimeter and characterization of photomultipliers. Master's thesis, IMAPP Master Degree, 2024.